Advances in Concrete Construction, *Vol. 10, No. 1 (2020) 61-69*
DOI: https://doi.org/10.12989/acc.2020.10.1.061

Influence of the shape of head anchors on the durability of reinforced concrete elements

M. José Martínez-Echeverría[1], Luisa María Gil-Martín*[2], José Rodríguez Montero[1] and Enrique Hernández-Montes[2]

[1]*Department of Construction Engineering and Engineering Projects, University of Granada (UGR), Campus Universitario de Fuentenueva s/n, 18072 Granada, Spain*
[2]*Department of Structural Mechanics, University of Granada (UGR). Campus Universitario de Fuentenueva s/n. 18072 Granada, Spain*

(*Received March 5, 2020, Revised July 1, 2020, Accepted July 7, 2020*)

Abstract. This paper looks into how the shape of headed bars may influence the durability of reinforced concrete structures. Nowadays the only heads used in site works are cylindrical in shape. An alternative shape of head is studied in this piece of work. The new head reduces the concentration of stresses and so the appearance of cracks. In this work durability is studied based on both, first cracking and failure mode. An experimental campaign of 12 specimens and finite element modelling are described. The specimens were subjected to an accelerated corrosion process using an electrical current supply. Direct current was impressed on the specimens until breaking. Test results and the results obtained from numerical models are presented. Results are presented in term of comparison between the two shapes of heads studied. It was shown that the shape of the head has a significant influence on durability of reinforced concrete structures with headed reinforcing bars.

Keywords: headed bars; shape of the heads; durability; anchorage

1. Introduction

Headed bars in reinforced concrete structures are used in heavily reinforced zones in order to reduce the development length of reinforcing bars, which result in a decongestion of the anchorage zone. Moreover, headed reinforcement presents lower slip, improves confinement in the nodes and enhances the response to cyclic loadings. The anchorage in a headed bar partly involves bearing the head against concrete, leading to an important reduction of the development length of the rebar.

Although the ACI 318 (2019) addresses the use of headed reinforcement, there is no provision in the Eurocode 2 (EC2) (European Committee for Standardization 2013) regarding the use of bars with heads. However, EC2 (§8.8) (European Committee for Standardization, 2013) suggests that large diameter bars "should be anchored with mechanical devices".

EC2:4-2 (CEN/TS 1992-4-2:2009, 2009) allows the use of cast-in headed bars to anchor the concrete by means of tension, shear or a combination of both as long as they have an ETA (European Technical Approval) or certification to demonstrate its usefulness for the intended use and assuring that the anchor has been rigorously tested. A study of the failure modes of the anchorage of headed bars under tension according to both (ACI-318, 2019) and EC2:4-2 (2009) can be found in Gil-Martín and Hernández-Montes (2019). The optimum embedment depth for headed anchors was recently investigated by Delhomme *et al*. (2016) based on tension tests of anchor rods.

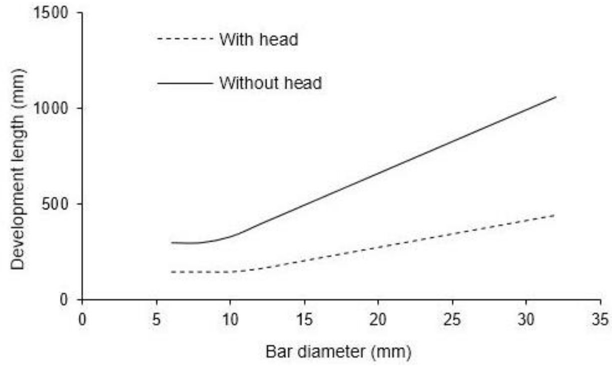

Fig. 1Development length of a deformed bar in function of its diameter for f_c'=30 MPa and f_y=400 MPa. Adapted from (Gil-Martín and Hernández-Montes 2019)

The ACI-318 (2019) code allows the use of heads to anchor deformed bars in tension if several conditions are fulfilled regarding bottom and side concrete covers, spacing between bars, yield strength (f_y≤420 MPa), bar size (ϕ_{bar}≤36 mm) and concrete compressive cylinder strength (f'_c≤40 MPa). The ACI-318 (2019) (§25.4.4) establishes a minimum area for the net bearing area of the head, A_{brg}, which must be at least four times the area of the bar, A_b. Fig. 1 shows the development length of a deformed bar according to (ACI Commitee 318, 2019) as a function of its diameter for f_c'=30 MPa and f_y=400 MPa.

From Fig. 1 it is evident that the development length can be significantly reduced if headed bars are used.

*Corresponding author, Professor
E-mail: mlgil@ugr.es

http://www.techno-press.org/?journal=acc&subpage=7
ISSN: 2287-5301 (Print), 2287-531X (Online)

(a)

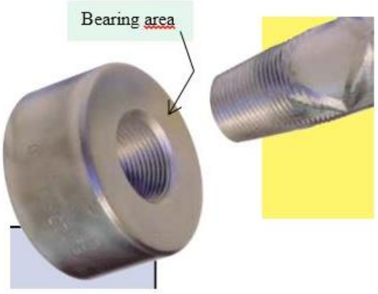

(b)

Fig. 2 Headed bars. (a) adapted from www.hrc-usa.com (b) adapted from www.erico.com (Lenton® brand product)

The heads can be welded, fattened (Fig. 2(a)) or threaded (Fig. 2(b)), the latter option being the most advantageous from the standpoint of handling, since the bars can be transported and tied without the heads (to be put in place at the end of the process).

Anchorage of the reinforcement using heads has been widely investigated (Hawkins 1968, Furche and Eligehausen 1992, Bashandy 1996, DeVries 1996, Thompson *et al*. 2002). The efficiency of this type of anchoring has been studied both experimentally and through numerical methods, mainly analysing the behaviour of the bar subjected to extraction-pull-out type tests. However, as far as the authors know, until now no study has explored how the shape of the head affects the durability of the RC member.

Traditionally, the head was cylindrical in shape (see Fig. 2), implying the existence of a flat contact surface with concrete and corners where concentration of stresses exists. Such stress concentrations could produce cracks, thereby accelerating the deterioration of the concrete cover (Fig. 3).

Durability is a great challenge in the scientific world of concrete structures (Mehta and Burrows 2001), and important technological advances have been made in this direction.

In the case of concrete structures, durability is not a matter of the concrete itself, whose deterioration is uncommon. To the contrary, problems related to the durability of a concrete structure are most likely caused by corrosion of the steel reinforcing bars (Coccia *et al*. 2016), which according to Fang *et al.* (2004) leads to: cracking in the cover concrete, reduction of the cross-sectional area of reinforcing bars, and loss of bond between concrete and reinforcements. The latter is the most critical factor according to Auyeung (2001).

It is well known that the corrosion of the rebars is one

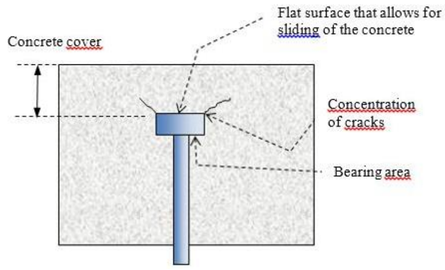

Fig. 3 Potential drawback of cylindrical heads

of the most relevant factors affecting degradation, causing problems and loss of bearing capacity in RC structures (Imperatore *et al.* 2012, Malerba *et al.* 2017). The effects of the corrosion not only reduces the diameter of the rebar, but can also affect the material constitutive relationship (Ouglova *et al.* 2006).

Corrosion products provoke an increase in volume of the rebar, which is equivalent to apply an outward pressure on the surrounding concrete. This pressure leads to cause the cover cracking. Once cracks appear, the process of corrosion is accelerated due to the greater level of exposure of the reinforcement to aggressive agents.

Because chemical adhesion is almost lost in corroded reinforcement, in corroded deformed rebars bond is mainly due to mechanical friction between ribs and concrete (Imperatore *et al.* 2012). In the case of the headed bars, whose anchorage relies mainly on bearing of the head - instead of the development length, the loss of bond strength due to corrosion may not play such a critical role in the durability of the RC member.

In practice, heads are cylindrical (see Fig. 2). As stated before, the shape of this head itself, with smooth surfaces and corners, together with the rust layer generated during the corrosion can cause cracking and spalling of the concrete cover (Fig. 3). In this work a new shape of head is studied: the hemispherical one. The new head has not outer flat surface in contact with concrete, which can improve the mechanical behaviour of the anchor due to both shrinkage of the surrounding concrete and reduction of stress concentration at the head edges.

The aim of this study was to assess the influence of the shape of the head upon the durability of the structural member. In this work durability is studied based on both, first cracking and failure mode. Following (Mangat and Elgarf 1999), an experimental study is carried out in which bond deterioration is induced by an accelerated corrosion process in the reinforcement using direct current.

In this work, two shapes of the head: cylindrical (the traditional one) and hemispherical and two sizes of rebar (12 and 25 mm diameters, respectively) have been studied.

A comparative study of the behaviour of two types of studied heads is presented.

Specimens with the same rebar diameter were tested simultaneously. Each series of six specimens underwent a process of accelerated corrosion by direct current (DC) in a saline environment. In each series, three specimens of each type of head were tested (i.e., three specimens with hemispherical heads and another three with cylindrical ones).

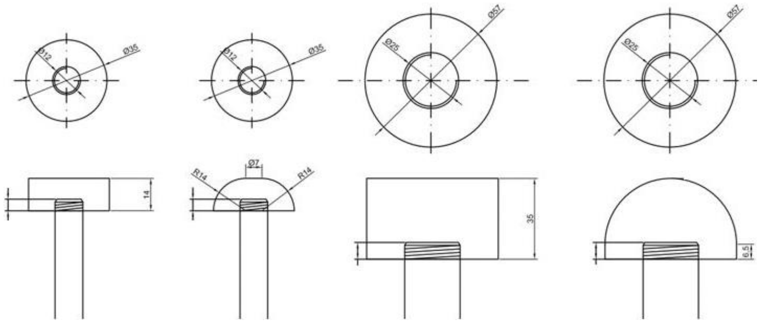

Fig. 4 Dimensions of the studied head bars (all dimensions are in mm)

(a) Studied head bars (b) Placement in moulds (c) Final specimens

Fig. 5 Specimens

Table 1 Concrete mixture proportions

Mixture composition of concrete specimens (kg/m^3)					Ratio of water/cement
Cement	Sand	Gravel	Water	Plasticizing admixture	
300	968	978	180	0.9	0.60

Table 2 Denomination of specimens, bearing areas of the rebar cross-section

Specimens	1C-12 2C-12 3C-12	1S-12 2S-12 3S-12	1C-25 2C-25 3C-25	1S-25 2S-25 3S-25
A_{brg} (mm^2)	849		2060.9	
A_b (mm^2)	113		490.9	

The behaviour of the tested heads has also been numerically simulated using 3D Finite Element (FE) models. Jebara *et al.* (2016) carried out 3D numerical analysis of single headed stud anchors and concluded that numerical model agreed well with experimental results.

2. Description of the specimens

To study the influence of shape, both cylindrical and hemispherical heads were threaded (3-4 threads) to rebars of 12 and 25 mm diameter. The dimensions of the heads are summarized in Fig. 4. Headed bars were placed in moulds before the concrete cast, the concrete covers at both sides and behind the head being twice the diameter of the rebar. All specimens were properly compacted to exclude the existence of cavities.

In order to protect the concrete-air interface, the rebars were painted with epoxy resin, except the head and 45 mm from the head. Both rebars and heads were made of standardized products. In all cases, the corrugated bars were made of steel with f_y=400 MPa (UNE 36068:2011, 2011), a common steel reinforcing bars used in reinforced concrete construction. The heads are made of carbon steel 1.1191 (UNE-EN 10083-1:2008, 2008), which is a structural steel for general use, weldable and widely used for pieces with a resistance ranging between 650 and 800 MPa and whose chemical composition in weight, according to the supplier, is 0.45% C and 0.65% Mn.

The concrete mixture proportions are reported in Table 1. The cement used was Portland CEM II/A-V 42.5 R and the aggregates were dolomitic sand and gravel with a maximum size of 16 mm. The slump cone of the fresh concrete was 9 cm and the 28-day compressive strength of the concrete was 34 MPa (measured on 150×300 mm cylindrical specimens).

Fig. 5 displays the studied head bars, their placing in the moulds and the final specimens.

All the specimens were covered with plastic and removed from their moulds the day after concreting. They were cured at room temperature in a room with 100% relative humidity for 28 days after casting.

Then the specimens were kept under dry conditions for a week, until starting the corrosion test to which specimens were subjected. The specimens (headed bar embedded in a cube of concrete) were subjected to an accelerated corrosion process in order to induce cracking. The corrosion test was kept until specimens were seriously damaged (from visual inspection).

A total of 12 specimens were tested. The denomination of each is a number followed by C (cylindrical) or S (hemispherical) depending on the shape of the head, and the diameter of the rebar. Table 2 shows the name of the specimens and both the area of the rebar and the bearing area of the head, A_b and A_{brg} respectively. As can be seen, the ratio A_{brg}/A_b is greater than 4 for all the specimens, following the ACI-318 (2019) prescription for the use of

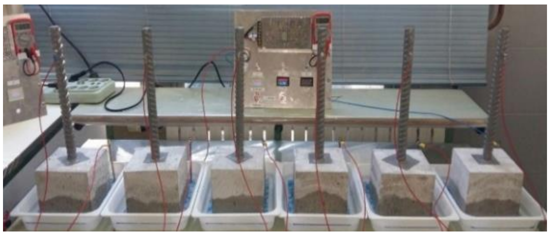

Fig. 6 General view of the accelerated corrosion process of C-25 and S-25 specimens

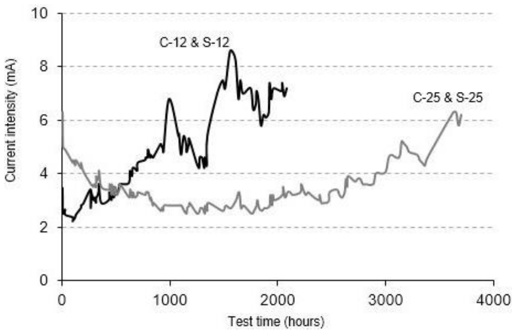

Fig. 7 Impressed current evolution

headed bars in tension.

3. Accelerated corrosion tests

In order to accelerate steel corrosion different techniques exist. A discussion of the most widely used techniques to accelerate steel corrosion in laboratories can be found in Malumbela *et al.* (2012).

In this work an impressed current technique was used. This technique has been widely used in concrete durability tests to obtain corrosion results within a reasonable period of time (El-Maaddawy and Soudki 2003, Ibrahim *et al.* 2018, Zhang *et al.* 2019).

An electrochemical potential was induced between the reinforcing steel embedded in concrete, which acted as the anode, and a stainless steel plate under the concrete cube, used as the cathode. Each test specimen was placed in a container with 3% NaCl solution to a level of 2 cm to allow for chloride penetration and to increase the electrical conductivity between the anode and the cathode. The current was impressed on the steel reinforcing bars by means of two 24 V power supplies, one per group of rebars with the same diameter. The test specimens were connected in series in order to guarantee that the same impressed current passed through by the six specimens of the group (Fig. 6).

Both the intensity of the current and the potential supplied by the source were monitored and daily recorded. The current intensity varied during the test due to different factors (temperature, chlorides penetration, initial cracking process) as can be seen in Fig. 7.

The current flow was converted to metal loss by using the Faraday`s law (Eq. (1)).

$$\Delta m = \frac{M \cdot I \cdot t}{z \cdot F} \tag{1}$$

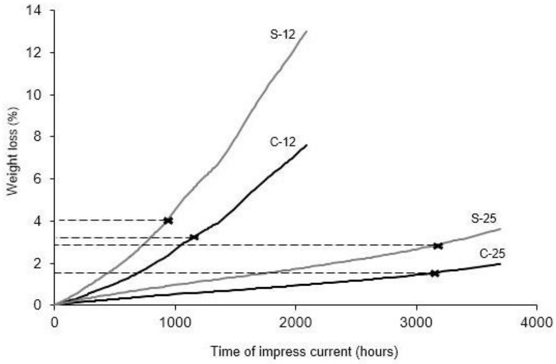

Fig. 8 Average steel weight evolution and first cracking

Table 3 Specimens weight loss (%) at time when the first surface crack appeared

Specimen	Weight loss (%)	Specimen	Weight loss (%)
1C-12	3.35	1C-25	1.70
2C-12	3.35	2C-25	1.45
3C-12	6.10*	3C-25	1.70
1S-12	4.05	1S-25	2.65
2S-12	4.05	2S-25	3.12
3S-12	4.05	3S-25	3.50

* Discarded specimen due to excessive deviation in its group

with Δm being the mass of steel consumed (in *g*), *M*= atomic weight of metal (equal to 56 for *Fe*), *I*=current intensity (in *A*), z=ionic charge (equal to 2), *t*=time (in *s*) and *F*=Faraday´s constant (equal to 96.500 A·s).

Because the set up was identical for the six corrosion specimens of each group (see Fig. 6), the amount of current consumed for water hydrolysis has been considered identical in all the specimens. That is, it is assumed that the effect of water hydrolysis is the same for all the specimens of identical dimensions regardless of the shape of the head. Accordingly, it has been neglected in the comparative study presented here.

The steel weight loss, defined as the quotient between the metal loss given by Eq. (1) and the initial mass of the embedded steel (i.e., the mass of the head plus the part of the rebar inside the concrete cube), has been calculated for each specimen.

Close, daily visual inspection of the state of the test specimens was carried out to detect the appearance of cracks. Table 3 summarizes the weight loss at the time when the first surface cracks appeared. It can be seen that the cracks appeared almost for the same weight loss in identical specimens, despite the dispersion associated with this type of measurements. Because measurements corresponding to specimen 3C-12 significantly differ from that of the other two samples of the same sort (i.e., 1C-12 and 2C-12), this specimen has not been considered.

The average weight loss evolution has been represented as a function of time, *t*, in Fig. 8.

Results in Fig. 8 and Table 3 show that the weight loss (in percentage of the initial mass of the embedded steel, i.e., head plus portion of rebar inside the concrete cube) necessary to cause first cracking is higher in the case of

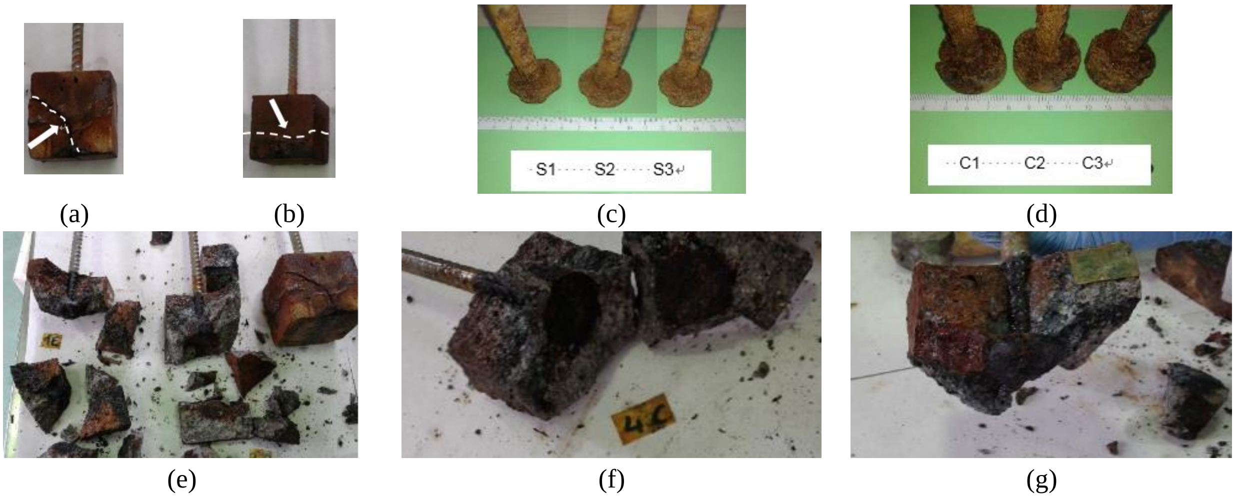

Fig. 9 Rebars of 12 mm diameter. (a) main crack in hemispherical heads (specimen 3S-12); (b) main crack in cylindrical heads (specimen 2C-12); (c) corroded bars with hemispherical heads; (d) corroded bars with cylindrical heads; (e) break of the concrete cube surrounding the heads (specimens 1S-12, 1C-12 and 3S-12); (f) observed mode of failure associated with cylindrical heads (specimen 4C-12); (g) observed mode of failure associated with hemispherical heads (specimen 3S-12)

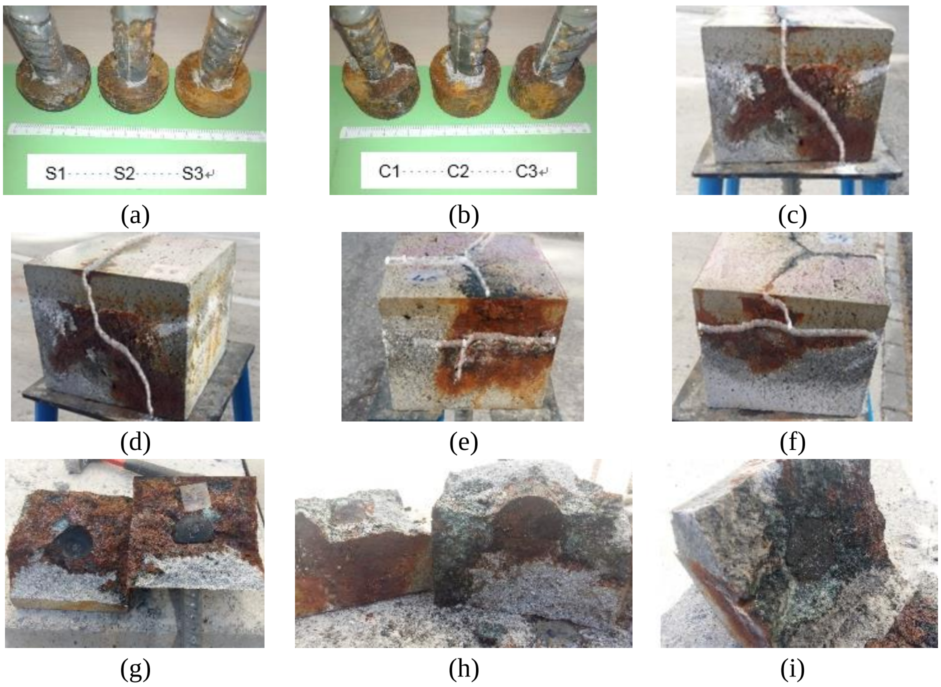

Fig. 10 Rebars of 25 mm diameter. (a) corroded bars with hemispherical heads; (b) corroded bars with cylindrical heads; (c) main crack in specimen 1S-25; (d) main crack in specimen 3S-25; (e) main crack in specimen 2C-25 (side 1); (f) main crack in specimen 2C-25 (side opposite 1); (g) observed mode of failure of specimen 5S-25; (h) observed mode of failure of specimen 1C-25; (i) observed mode of failure of specimen 3C-25

hemispherical heads than in the case of traditional ones (cylindrical). In term of time, Fig. 8 shows that surface first cracking appears earlier in the case of 12 mm diameter hemispherical heads and almost at the same time for both types of heads in the case of 25 mm diameter rebars.

Corrosion stains were detected on the specimens before cracking. Both stains (brown coloured) and cracks appeared first in specimens with cylindrical head.

In all the tested specimens, cracking starts at the centre of the base of the specimens in contact with the stainless steel plate used as cathode. Over time, these micro-cracks were both lengthening and widening until reach the edge of the concrete cubes. However, once these first cracks affect the full width of the samples, the new cracks present different patterns for both types of heads. In the case of the cylindrical heads, the propagation of the crack is perpendicular to the base but after about 2-3 cm a sudden change of direction happens (see Figs. 9(b), 10(e) and 10(f)) and cracks propagate parallel to the side of the cube at the level of the external side of the head (see Fig. 10(i)). On the other hand, in the case of hemispherical specimens crack also propagate perpendicularly to the base but after 3-4 cm it suffers an erratic change of direction. This inclined crack propagates indistinctly toward the opposite face (see Figs. 10(c) and 10(d)) or to the lateral side of the concrete cube (as in Fig. 9(a)). As the level of corrosion progresses, concrete deterioration was greater due to the widening of cracks.

The corrosion process was halted simultaneously for all the specimens of each series (one series per rebar diameter) when the widths of the cracks in the surface of all the concrete cubes were large enough to consider that specimens were burst. At that point, each specimen was broken and further examined.

4. Breakage of the corroded specimens

The specimens were subjected to an accelerated corrosion process, as explained in the previous section, until the width of the cracks was so large that all the specimens of the series were burst (see Figs. 9(a) and 9(b)). At that moment, the corrosion-induced test was stopped and the concrete surrounding the rebar was removed manually, using a hammer (Figs. 9(c) and 9(d)).

The pictures in Fig. 9 correspond to 12 mm diameter rebars. At first glance, it was evident that corrosion had rounded the edge that delimited the bearing area in spherical heads-where the thickness was minimum (see Fig. 9(c)). In the case of the cylindrical ones (Fig. 9(d)), the reduction of the bearing diameter of the head was less evident, but in this case wide cavities in the heads appeared, induced by corrosion. The concrete was found to come off more easily with the blow of the hammer in the case of the cylindrical heads. Regarding the failure mode, the cylindrical heads were separated from concrete by a smooth surface at the level of the outside part of the head (Figs. 9(e) and 9(f)), whereas no plane of weakness appeared among the hemispherical ones (Fig. 9(g)). Findings were similar for the specimens with 25 mm diameter rebars. The noteworthier pictures corresponding to rebar of 25 mm are offered in Fig. 10.

Figs. 10(a) and 10(b) respectively show the hemispherical and cylindrical headed bars after the corrosion process. The dark brown surface due to corrosion was more evident on the smaller specimens. Again, the concrete came off the cylindrical ones more easily under the blow of the hammer. The main cracks in specimens with hemispherical heads (1S-25 and 3S-25) are indicated in Figs. 10(c) and 10(d), respectively. In Figs. 10(e) and 10(f), the main cracks in specimen 2C-25 on opposite lateral sides reveal the existence of a plane of weakness in the outer part of the cylindrical head. Such a plane of weakness does not appear in the spherical heads, as can be seen in Fig. 10(g). The mode of failure in the cylindrical bars is the one that appears in Figs. 10(h) and 10(i), where, as in the case of the 12 mm diameter bars, the plane of rupture develops at the level of the outermost side of the head.

5. Numerical analysis

As Ayinde *et al.* (2019) did, numerical analysis is used to study the effect of corrosion.

Numerical thermo-mechanical analysis of the tested specimens was carried out. Given their symmetry, just half of each specimen was modelled (Fig. 11(a)). For the sake of simplicity, both the rebar and the head are assumed to be made of the same material.

The model has been meshed with hexahedral-shaped 3D solid elements automatically generated. The mesh density has been stablished after some iterations based on the convergence of the solution.

Both, steel and concrete have been considered elastic, homogeneous and isotropous materials. A bilinear constitutive model has been considered for the steel elements (i.e., reinforcing bars and heads). For concrete in compression, the nonlinear uniaxial model produced by EC2 (European Committee for Standardization 2013) is adopted. In order to model cracking, the tensile strength of concrete is considered. For convenience in the numerical analysis, the stress-strain relationship for concrete in tension is characterized by linear strain-softening in which the tensile stress is gradually reduced to zero at increasing strain.

The most important parameters of both materials (steel and concrete) are summarized in Table 4. As allowed under the regulations for simplified calculations, a safe constant value of the thermal conductivity was considered for both steel and concrete; here, the value was fictitiously multiplied by 100 in order to simulate the effect of corrosion. As Ghojel (2004) did, a conductance of 100 W/m^{2}K was considered for the contact.

Even when the weight loss is not homogeneous because the corrosion products are distributed throughout the concrete pores (Zhao *et al.* 2011), for the sake of simplicity and in line with that other researchers did (Chernin *et al.* 2010, Kim *et al.* 2010, Lu *et al.* 2011), a uniform distribution of rust layer around steel rebar has been

Table 4 Properties of concrete and steel

Material	Property	20°C (+273 K)
concrete	f_{cm} [MPa]=f_{ck}+8	33
	Tensile Strength [MPa]	2.56 *
	Elastic modulus, E_{cm} [MPa]	$3.148\cdot10^{4}$ *
	ε_{c1} [%] – strain at peak stress-	0.21
	Poisson´s ratio	0.2
	Thermal expansion coefficient [K^{-1}]	$10\cdot10^{-6}\cdot10^{-2}$ **
	Specific heat [J/KgK]	1000
	Thermal conductivity [W/mK]	1.6
steel	f_y [MPa]	400
	Elastic modulus, E_s [MPa]	$2\cdot10^{5}$
	Poisson's ratio	0.3
	Thermal expansion coefficient [K^{-1}]	$12\cdot10^{-6}$
	Specific heat [J/KgK]	600
	Thermal conductivity [W/mK]	$45\cdot10^{2}$ ***

* According to EC2 [2];
** Actual value divided by 100
*** Actual value multiplied by 100

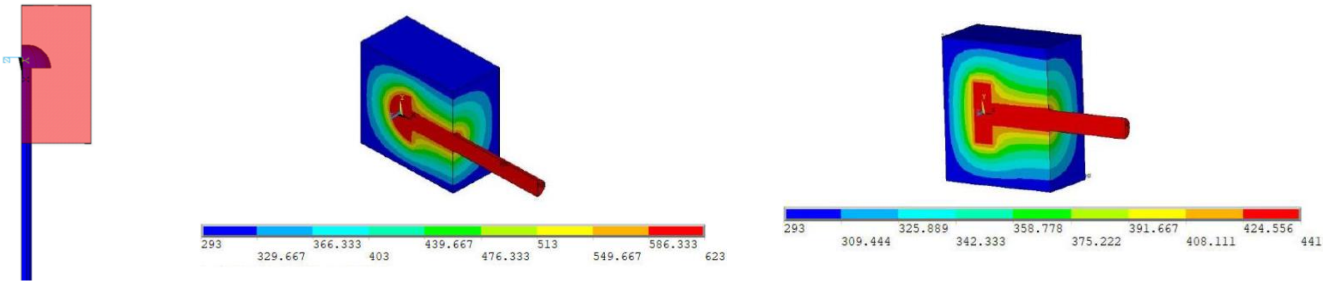

(a) (b) (c)

Fig. 11 Numerical model. (a) model corresponding to hemispherical head embedded in concrete cube; (b) temperature field from thermal analysis for S-25 specimens; (c) temperature field from thermal analysis for C-12 specimens

considered in this study.

In the numerical models (Ayinde *et al.* 2019, Zhou *et al.* 2019), the outward pressure on the surrounding concrete (i.e., around the rebar and against the concrete) due to the increase in volume during corrosion has been simulated by applying an increase of temperature at the embedded rebar, which results in an expansion of the steel.

In the thermal analysis, a linear heat flow with no mass transport effects is considered. Temperature has been gradually increased until generating significant crushing and cracking levels around the rebar. The applied temperatures to specimens verify that the temperature/rebar diameter ratio is the same for both series. The maximum applied temperatures were 350ºC and 168ºC (+273 K), respectively for the 25 mm and 12 mm diameter rebar. Heating was applied to all nodes located at the end of the bar while a reference temperature of 20ºC (+273 K) was stablished at the external surfaces of the concrete cube.

Temperatures in each node of the model obtained from the thermal analysis (Figs. 11(b) and 11(c)) constituted the only load considered for the mechanical study, in which three-dimensional solid element types were used to model both concrete and steel and for both, thermal and mechanical analysis. Results obtained from thermal analysis corresponding to 12 mm rebar and for both shapes of head are presented in Figs. 11(b) and 11(c).

As stated earlier, both the head and rebar were assumed to be of the same material (f_y=400 MPa), and a bilinear kinematic hardening model (defined by the yield stress and the hardening modulus of elasticity) was used to define the strain-stress curve of steel. The concrete is modelled by an eight-node brick element capable of simulating the cracking and crushing behaviour of concrete. This element is based on the Willam and Warnke (1975) failure criterion being cracking and crushing defined by a failure surface depending on whether the principal stress is tensile or compressive respectively.

In the mechanical model the expansion coefficient of concrete was fictitiously divided by 100 in order to impose that only steel expands during the simulated corrosion process.

The effect of reinforcement corrosion on bond properties has been widely studied using FE models and pull-out tests (Reinhardt *et al.* 1984, Lee *et al.* 2002) and is out of the scope of this study.

Fig. 12 depicts crushing and first cracks obtained through FE analysis for each specimen.

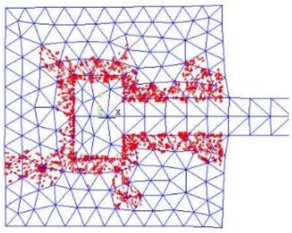

(a) failure areas in C-25 specimen

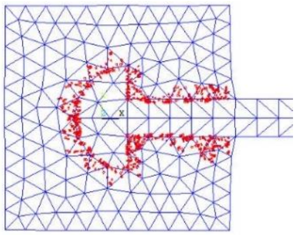

(b) failure areas in S-25 specimen

Fig. 12 Numerical model

Fig.12 corresponds to 25 mm diameter rebar when a temperature of 350ºC is applied to the model.

Fig. 12 displays points where failure of concrete has been reached, either by crushing or by cracking. This figure shows different failure pattern in both heads. The volume of affected concrete in the surrounding of the head is bigger in the case of cylindrical head than in the hemispherical one. Comparison of both figures in Fig. 12 also shows that the concentration of damaged concrete in the surfaces of the head in contact with concrete is higher in the case of the cylindrical head. The above may cause loss of bond between concrete or even the split of the concrete around the reinforcing bar. Moreover, in Fig. 12 can be observed that the elements of the mesh affected by cracking/crushing define planes of weakness that propagate from the corners of the cylindrical head, where stress concentrations exist, to the edges of the specimen.

In Fig. 12(a) it is evident that cracks propagate from the external perimeter of the cylindrical head, generating a flat breaking surface consistent with experiments (see Figs. 10(h) and 10(i)). The level of damage in Fig. 12(b), hemispherical head, seems to be smaller.

The above is in line with the experimental evidences depicted in the pictures of Figs. 9 and 10 in which concrete in the outside part of the cylindrical head could be easily separated from the steel by a blow of the hammer.

Numerical results confirm that observed in the experimental campaign; that is, that the shape of the heads plays an important role in the growth of existing micro-cracks.

It is interesting to note that stress concentration at corners, owing to other effects such a shrinkage, is not dealt with in this paper. Such stress concentration, however, is known to generate critical zones involved in the onset of crack propagation.

5. Conclusions

Two types of heads of reinforcing headed bars were used to investigate the influence of the shape of the head in the durability of RC members. Comparisons were made based on both experimental results and finite element models. This study reached the following conclusions:

- According to the results of accelerated corrosion process presented in this work, the loss weight for which first crack appears at the surface of concrete is higher in the case of hemispherical head than in the cylindrical one. The above evidence a better behaviour of the first shape of head.
- Crack propagation is indeed highly influenced by the shape of the head, leading to different failure modes. Cylindrical heads tend to break along a flat plane defined by the outermost surface of the head. No similar weakness plane is apparent in the case of the hemispherical heads.
- The reduction of damage in the cover could translate into a rise in durability of the RC structures with hemispherical headed bars.
- Numerical models results, in which the increase of volume of the steel since the corrosion has been simulated by heating of embedded steel, are in line with the experiments and confirm the influence of the shape of the head in the durability of the RC member.
- New head shapes might therefore be designed with the aim of reduce the stress concentration and in view of the influence of the head shape in the failure mode. More research is necessary in order to discover the more suitable head that satisfies both durability and ergonomic (ease of handling in site) requirements.

Acknowledgements

Authors thank the support of ERSI group during the development of this research. The authors gratefully acknowledge the contribution of Prof. J.F. Carbonell-Márquez from the University of Córdoba in developing the FE models presented in this paper. The authors would also like to thank Laboratory Engineer Andrés Gil for his help during the casting and testing operations.

References

ACI 318 (2019), Building Code Requirements for Structural Concrete and Commentary. Detroit: American Concrete Institute, ACI, Farmington Hills, MI, USA.

Auyeung, Y. (2001), "Bond properties of corroded reinforcement with and without confinement", Ph.D. Dissertation, The State University of New Jersey, New Brunswick

Ayinde, O.O., Zuo, X.B. and Yin, G.J. (2019), "Numerical analysis of concrete degradation due to chloride-induced steel corrosion", *Adv. Concrete Constr.*, **7**(4), 203-210. https://doi.org/10.12989/acc.2019.7.4.203.

Bashandy, T.R. (1996), "Application of headed bars in concrete members", Ph.D. Dissertation, University of Texas, Austin.

Chernin, L., Dimitri, V.V. and Volokh, K.Y. (2010), "Analytical modelling of concrete cover cracking caused by corrosion of reinforcement", *Mater. Struct.*, **43**, 543-556. https://doi.org/10.1617/s11527-009-9510-2.

Coccia, S., Imperatore, S. and Rinaldi, Z. (2016), "Influence of corrosion on the bond strength of steel rebars in concrete", *Mater. Struct.*, **49**, 537-551. https://doi.org/10.1617/s11527-014-0518-x.

Delhomme, F., Roure, T., Arrieta, B. and Limam, A. (2016), "Pullout behavior of cast-in-place headed and bonded anchors with different embedment depths", *Mater Struct.*, **49**(5), 1843-1859. https://doi.org/10.1617/s11527-015-0616-4.

DeVries, R. (1996), "Anchorage of headed reinforcement in concrete", Ph.D. Dissertation, University of Texas, Austin.

El-Maaddawy, T.A. and Soudki, K.A. (2003), "Effectiveness of impressed current technique to simulate corrosion of steel reinforcement in concrete", *J. Mater. Civil Eng.*, **15**(1), 41-47. https://doi.org/10.1061/(ASCE)0899-1561(2003)15:1(41).

Eurocode 2 (2009), Design of fastening for use in concrete. Part4-2: Headed Fasteners, European Committee for Standardization; Brussels, Belgium.

Eurocode 2 (2013), Design of Concrete Structures. Part 1–1: General Rules and Rules for Buildings, European Committee for Standardization, Brussels, Belgium.

Fang, C., Lundgren, K., Chen, L. and Zhu, C. (2004), "Corrosion influence on bond in reinforced concrete", *Cement Concrete Res.*, **34**(11), 2159-2167. https://doi.org/10.1016/j.cemconres.2004.04.006.

Furche, J. and Eligehausen, R. (1991*), Lateral Blow-out Failure of Headed Studs Near a Free Edge*, ACI Special Publications (ACI SP-130), Stuttgart, Germany, pp. 235-252. http://dx.doi.org/10.18419/opus-432.

Ghojel, J. (2004), "Experimental and analytical technique for estimating interface thermal conductance in composite structural elements under simulated fire conditions", *Exp. Therm. Fluid Sci.*, **28**(4), 347-354. https://doi.org/10.1016/S0894-1777(03)00113-4.

Gil-Martín, L.M. and Hernández-Montes, E. (2019), "Reinforcement anchored in tension by heads. Review of capacity formulation and applicability limits", *Eng. Struct.*, **184**, 186-193. https://doi.org/10.1016/j.engstruct.2019.01.063.

Hawkins, N.M. (1968), "The bearing strength of concrete loaded through rigid plates", *Mag. Concrete Res.*, **20**(62), 31-40. https://doi.org/10.1680/macr.1968.20.62.31.

Ibrahim, M.A., Sharkawi, A.E.M., El-Attar, M.M. and Hodhod, O.A. (2018), "Assessing the corrosion performance for concrete mixtures made of blended cements", *Constr. Build. Mater.*, **168**, 21-30. https://doi.org/10.1016/j.conbuildmat.2018.02.089.

Imperatore, S., Leonardi, A. and Rinaldi, Z. (2012), *Mechanical Behaviour of Corroded Rebars in Reinforced Concrete Elements*, Springer, Berlin, Heidelberg, Germany, **61**, 207-220. https://doi.org/10.1007/978-3-642-24638-8_13.

Jebara, K., Ožbolt, J. and Hofmann, J. (2016), "Pryout failure of single headed stud anchor: 3D numerical FE analysis", *Mater. Struct.*, **49**(11), 4551-4563. https://doi.org/10.1617/s11527-016-

0806-8.
Kim, K.H., Jang, S.Y., Jang, B.S. and Oh, B.H. (2010), "Modeling mechanical behavior of reinforced concrete due to corrosion of steel bar", *ACI Mater. J.*, **107**(2), 106-113.
Lee, H.S., Noguchi, T. and Tomosawa, F. (2002), "Evaluation of the bond properties between concrete and reinforcement as a function of the degree of reinforcement corrosion", *Cement Concrete Res.*, **32**(8), 1313-1318. https://doi.org/10.1016/S0008-8846(02)00783-4.
Lu, C., Jin, W. and Liu, R. (2011), "Reinforcement corrosion-induced cover cracking and its time prediction for reinforced concrete structures", *Corros. Sci.*, **53**(4), 1337-1347. https://doi.org/10.1016/j.corsci.2010.12.026.
Malerba, P.G., Sgambi, L., Ielmini, D. and Gotti, G. (2017), "Influence of corrosive phenomena on bearing capacity of RC and PC beams", *Adv. Concrete Constr.*, **5**(2), 117-143. https://doi.org/10.12989/acc.2017.5.2.117.
Malumbela, G., Moyo, P. and Alexander, M. (2012), "A step towards standardising accelerated corrosion tests on laboratory reinforced concrete specimens", *J. S. Afr. Inst. Civil Eng.*, **54**(2), 78-85. http://hdl.handle.net/11427/27644.
Mangat, P.S. and Elgarf, M.S. (1999), "Bond characteristics of corroding reinforcement in concrete beams", *Mater. Struct.*, **32**(2), 89-97. https://doi.org/10.1007/BF02479434.
Mehta, K. and Burrows, R. (2001), "Building durable structures in the 21st century", *Concrete Int.*, **23**(3), 57-63.
Ouglova, A., Berthaud, Y., François, M. and Foct, F. (2006), "Mechanical properties of an iron oxide formed by corrosion in reinforced concrete structures", *Corros, Sci.*, **48**(12), 3988-4000. https://doi.org/10.1016/j.corsci.2006.03.007.
Reinhardt, H.W., Blaauwendraad, J. and Vos, E. (1984), "Prediction of bond between steel and concrete by numerical analysis", *Mater. Constr.*, **17**(4), 311-320. https://doi.org/10.1007/BF02479089.
Thompson, M.K., Jirsa, J.O., Breen, J.E. and Klingner, R.E. (2002), "Anchorage Behavior of Headed Reinforcement: Literature Review", FHWA/TX-0-1855-1, Research Report 1855-1, 00970589.
UNE 36068:2011 (2011), Ribbed Bars of Weldable Steel for the Reinforcement of Concrete.
UNE-EN 10083-1:2008 (2008), Steels for Quenching and Tempering - Part 1: General Technical Delivery Conditions.
Willam, K.J. (1975), "Constitutive model for the triaxial behaviour of concrete", *Proceedings of the International Association for Bridge and Structural Engineering*, Bergamo, Italy, **19**, 174-179.
Zhang, W., Chen, J. and Luo, X. (2019), "Effects of impressed current density on corrosion induced cracking of concrete cover", *Constr. Build. Mater.*, **204**, 213-223. https://doi.org/10.1016/j.conbuildmat.2019.01.230.
Zhao, Y., Hu, B., Yu, J. and Jin, W. (2011) "Non-uniform distribution of rust layer around steel bar in concrete", *Corros. Sci.*, **53**(12), 4300-4308. https://doi.org/10.1016/j.corsci.2011.08.045.
Zhou, X., Tu, X., Chen, A. and Wang, Y.. (2019), "Numerical simulation approach for structural capacity of corroded reinforced concrete bridge", *Adv. Concrete Constr.*, **7**(1), 11-22. https://doi.org/10.12989/acc.2019.7.1.011.

JK